Article

Synthesis of SnS_2 Ultrathin Nanosheets as Anode Materials for Potassium Ion Batteries

HU Rong[1#], FANG Yongzheng[1#], LIU Xiaoyu[2], ZHU Kai[1]✉
CAO Dianxue[1], YI Jin[2]✉ and WANG Guiling[1]✉

Received January 12, 2021
Accepted February 9, 2021

Potassium(K) ion batteries present their promising application for large-scale energy storage systems with cost-effective characteristic. Unfortunately, the large K ion radius results in sluggish K ion diffusion kinetics and volume expansion of the electrode during the K ion insertion/extraction process. It is a challenge to explore capable anode materials with remarkable K ion storage ability. Herein, we design and prepare SnS_2 ultrathin nanosheets *via* a facile hydrothermal process. When severing as anode materials for K ion batteries with optimized electrolyte, SnS_2 presents an improved capacity and rate ability. The capable electrochemical performance is ascribed to the reduced ion diffusion pathway and capacitor-dominated K-ion storage process. In addition, the K ion storage mechanism of SnS_2 is investigated by the *ex-situ* X-ray diffraction technique.

Keywords SnS_2; Electrolyte; Potassium ion battery; Anode

1 Introduction

Development and utilization of renewable energy sources for electronic energy generation make dramatic progress in recent decades[1,2]. For smart grid management, a large-scale energy storage system is a crucial factor to balance electronic energy generated in peak and off-peak periods[3,4]. Up to now, lithium-ion batteries, as the most successful batteries technology, have been widely applied in the electronic mobile equipment and electric vehicle[5,6]. However, they may not be the perfect candidate for the large-scale energy storage system because of the increasing price and the limited resource of lithium on the earth[7,8]. Thus, many researches about advanced batteries technology beyond lithium are conducted[9,10]. Potassium(K) ion batteries attract extensive attention owing to the abundant resources of K[11,12]. The potassium ion batteries also present a "rock chair" mechanism as lithium-ion batteries because of similar chemical behaviors of Li and K[13]. Moreover, the low redox potential of K/K^+(–2.93 V *vs*. SHE) promises a high working voltage of K ion batteries[14]. It should be noted that the batteries cost of production can be reduced by using Al current collector instead of Cu current collector because K-Cu alloy is not formed at low potentials[15]. Above advantages make K ion batteries be emerged as a competitive candidate for future energy storage system. Nevertheless, the commercial application of K ion batteries is impeded by insufficient electrode materials[16]. It is an austere challenge to exploring capable electrode material with improved capacity and remarkable rate ability.

Transition metal sulfides emerge as an appealing anode material for beyond lithium ion batteries due to the high theoretical capacity and good electronic conductivity[17]. Meanwhile, the metal-sulfur band with low activation energy is in favor of conversion reaction[18]. Among various metal sulfurs, SnS_2 is one of the most promising electrode material thanks to its large interlayer spacing and small toxicity[19]. However, the electrochemical performance of SnS_2 is restricted by the volumetric change during the metal ion intercalation/extraction process[20]. The violent volumetric change would lead to structural damage and active materials falling off from the current collector. Several strategies are developed to overcome the above issue. Sun *et al*.[21] synthesized the N-doped carbon nanoboxes encapsulated SnS_2 nanoparticles(SnS_2@C), which exhibited a high capacity (660 mA·h/g at 100 mA/g) and favorable cycling stability(a capacity retention of 88.6% after 100 cycles) in sodium ion batteries. The carbon modification serves as a volume buffer to promote the cycling stability of the anode[22]. Until now, nanostructuring would be the most available strategy to achieve the enhanced electrochemical performance of anode materials. Constructing nanomaterials would reduce inner stress and prevent structure cracking[23]. Meanwhile, it also brings the benefits of a short ion/electron transport pathway and a more active surface area[24]. Thus, it is desired to design and fabricate SnS_2 nanomaterials employing as electrode materials for K ion batteries.

Electrolyte engineering is a vital approach for designing high-performance battery. For the K ion batteries, the weak

✉ WANG Guiling
wangguiling@hrbeu.edu.cn
✉ YI Jin
jin.yi@shu.edu.cn
✉ ZHU Kai
kzhu@hrbeu.edu.cn
# These authors contributed equally to this work.
1. Key Laboratory of Superlight Materials and Surface Technology, Ministry of Education, College of Material Science and Chemical Engineering, Harbin Engineering University, Harbin 150001, P. R. China;
2. Institute for Sustainable Energy, College of Sciences, Shanghai University, Shanghai 200444, P. R. China

https://doi.org/10.1007/s40242-021-0017-x

Lewis acidity of K ion promises good mobility of K ion in the nonaqueous electrolyte and high ionic conductivity[25]. Recently, Ming's group[26] demonstrates that the side-effects from the electrolyte decomposition results in unstaisfied performance. The electrolyte decomposes and forms solid electrolyte interphase(SEI) on the anode[27]. A high-quality SEI film could protect the electrode materials and provide a fast and stable ion diffusion pathway[28]. The electrolyte optimization should be noticed for electrode materials application.

Herein, we design and synthesize SnS_2 nanosheets *via* a facile hydrothermal method. $SnCl_4{\cdot}5H_2O$, thioacetamide(TAA), and ethanol are used as raw materials to synthesize flaked-SnS_2 composed of extremely thin SnS_2 nanosheets hydrothermally. The uniform thin SnS_2 nanosheets are randomly gathered, leaving the void between each other. And the thickness of SnS_2 could be estimated to be *ca*. 8 nm based on the vertical sheets and wrinkled sheets. So far, the structure of ultra-thin SnS_2 nanosheet has rarely been reported. In the optimized electrolyte, SnS_2 as the anode of the potassium ion batteries(PIBs) presents an improved capacity and capable rate ability, and the mechanism is further analyzed from the perspective of SEI film. Meanwhile, the kinetics analysis demonstrates the capacitive contribution dominates the capacity, leading to stable cycling stability. This work presents a potential application of SnS_2 as a capable anode material for K ion batteries.

2 Experimental

2.1 Synthesis of Flake-SnS_2

$SnCl_4{\cdot}5H_2O$(0.35 g) and 1.50 g of TAA were mixed in 35 mL of ethanol under vigorously stirring for 2 h. Then, the obtained mixture was poured into a Teflon autoclave and solvothermally treated at 180 °C for 12 h. The yellow SnS_2 materials were obtained after centrifugation, washing with ethanol 4—5 times, and drying at 60 °C for 12 h.

2.2 Materials Characterization

The crystalline phase information and surface elemental states of materials were conducted by means of X-ray diffraction(XRD, Cu *Kα* radiation, Rigaku TTR Ⅲ, 5°—90° and 30°—55°) and X-ray photoelectron spectroscopy(XPS, Thermo ESCALAB 250 instrument), respectively. Scanning electron microscope(SEM) on a JEOL JSM7500F instrument and transmission electron microscope(TEM) on a JEOL JEM-2100 instrument measurements were carried to confirm the morphology and microstructural properties. The elemental analysis of the sample was acquired on an energy dispersive X-ray spectrometer(EDS).

2.3 Electrochemical Characterizations

The CR2032-type coin cell was assembled to analyze the electrochemical performance of flake-SnS_2 material. In terms of the slurry coating process of anode preparation, active materials(flake-SnS_2), Super P and sodium carboxymethyl cellulose(CMC) were mixed with the mass ratio of 7:2:1 and diluted with deionized water. The prepared slurry was then evenly coated onto the current collector of Cu foil and dried at 60 °C in a vacuum oven overnight. The completely dried pieces were punched into circles 12 mm in diameter, and the mass loading of active materials was approximately 1 mg/cm^2. The CR2032-type coin cell was assembled with the counter electrode of metal potassium pellet and the separator of glass fiber(Whatman GF/D) in a glovebox(Ar-filled, H_2O, and O_2 content<0.1 ppm). The influence of two electrolytes on the electrochemical performance of materials was investigated. The used electrolytes were 1 mol/L KPF_6 dissolved in the ethylene carbonated/dimethyl carbonate/diethyl carbonate (EC/DMC/DEC, volume ratio 1:1:1) togerther with 0.8 mol/L KPF_6 in EC/DEC(volume ratio 1:1), respectively. The cyclic voltammetry tests(CV, 0.25—2.35 V) and electrochemical impedance spectra(EIS) were carried on the Bio-Logic VMP3 electrochemical workstation. Galvanostatic charge/discharge tests were performed in a NEWARE battery testers (0.25—2.35 V).

3 Results and Discussion

The flake-SnS_2 can be obtained by a one-step hydrothermal route,where $SnCl_4{\cdot}5H_2O$, TAA, and ethanol are used as raw materials. The XRD analysis of the obtained SnS_2 sample is displayed in Fig.1(A). All the diffraction peaks of flake-SnS_2 can be indexed to the hexagonal SnS_2(JCPDS No.23-0677), showing sharp and clear peaks with a high intensity[29]. This confirms the good crystallinity of the prepared SnS_2. Considering the further study of the chemical state of flake-SnS_2, the XPS analysis of the sample was carried out. The survey spectrum of flake-SnS_2[Fig.1(B)] detects the presence of Sn and S elements. The high-resolution XPS spectrum of Sn_{3d}[Fig.1(C)] shows divided peaks at 494.6 and 486.2 eV, fitting into $Sn_{3d_{5/2}}$ and $Sn_{3d_{3/2}}$ of Sn^{4+}, respectively[30]. The XPS spectrum of S_{2p}[Fig.1(D)] can be devided into two typical peaks at 162.6 and 161.5 eV, representing $S_{2p1/2}$ and $S_{2p3/2}$ in Sn—S bonds, respectively, which implies the existence of S^{2-} in SnS_2[31]. These results further confirm the successful synthesis of SnS_2.

The morphology and microstructure of flake-SnS_2 were

https://doi.org/10.1007/s40242-021-0017-x

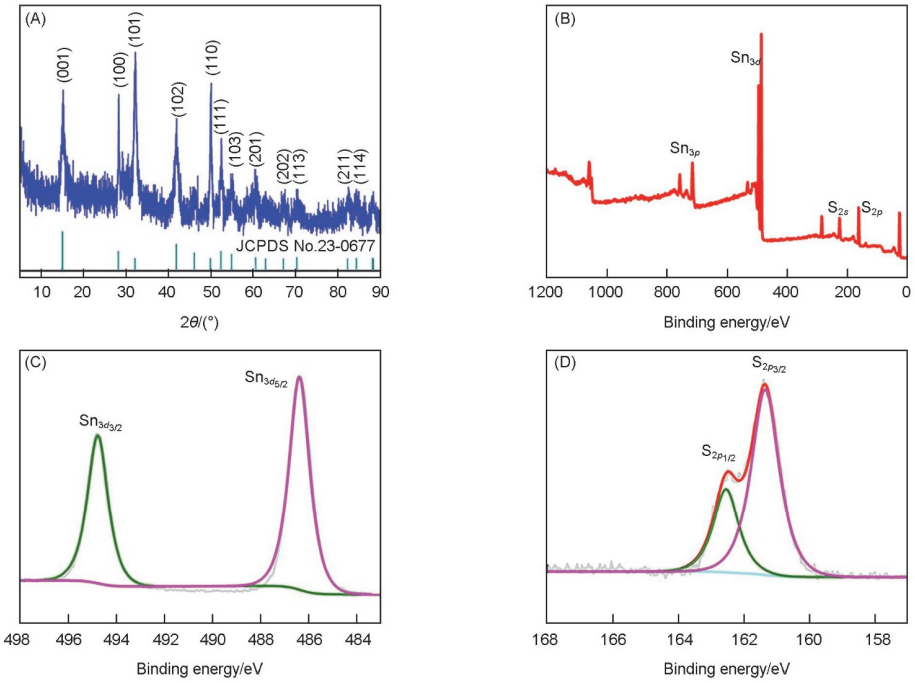

Fig.1 XRD patterns of flake-SnS_2(A), and XPS survey spectrum(B), high-resolution Sn_{3d}(C) and S_{2p}(D) XPS spectra of flake-SnS_2

confirmed by SEM and TEM analysis[Fig.2(A)—(E)]. From the SEM images of SnS_2[Fig.2(A) and (B)], it can be found that the micrometer-sized scaled flake-SnS_2 is composed of extremely ultrathin SnS_2 nanosheets, which can also be determined from the TEM image[Fig.2(C)]. The uniform thin SnS_2 nanosheets with *ca.*100 nm diameter are randomly gathered[Fig.2(D)], leaving the void between each other, which is conducive to provide an abound contact area with electrolyte. The thickness of SnS_2 could be estimated to be *ca.* 8 nm based on the vertical sheets and wrinkled sheets. The formation process of the unique, extremely thin flake-SnS_2 structure has been explored through the morphology at different hydrothermal reaction time. When the reaction started at 4 h[Fig.S1(A), see the Electronic Supplementary Material of this paper], a large number of very small SnS_2 nanosheets appeared in the solution of hydrothermal reaction. After 8 h[Fig.S1(B), see the Electronic Supplementary Material of this paper], the tiny SnS_2 nanosheets began to grow up and gradually aggregated into larger SnS_2 flakes. When the reaction continued to 12 h, a large number of micrometer-sized scaled SnS_2 flakes appeared [Fig.S1(C), see the Electronic Supplementary Material of this paper], and some individual SnS_2 nanosheets were retained[Fig.S1(D), see the Electronic Supplementary Material of this paper]. The high resolution transmission electron microscopy(HRTEM) images of flake-SnS_2[Fig.2(E)] exhibit two lattice fringes with lattice spacings of 0.598 and 0.278 nm, which are related to (001) and (101) planes of SnS_2, respectively. In addition, elemental mapping was studied to confirm the distribution of Sn and S elements in SnS_2. The uniform

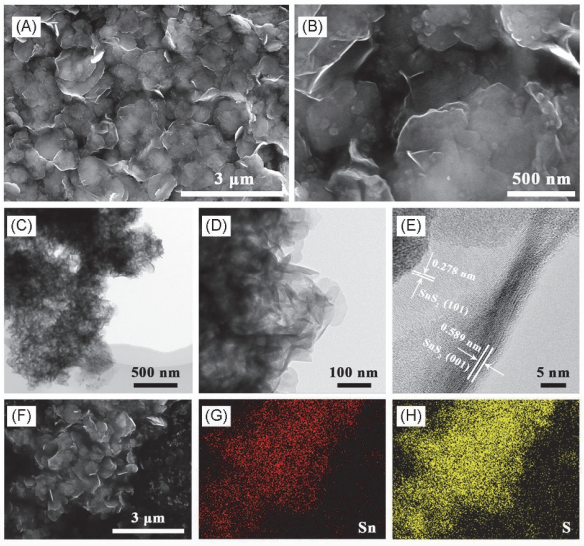

Fig.2 SEM images of flake-SnS_2(A, B), TEM(C, D), HRTEM(E), and EDS mapping(F—H) images of flake-SnS_2(Sn, S elements)

distribution of Sn(red) and S(yellow) in the SnS_2 sample further demonstrates the successful synthesis of flake-SnS_2.

To investigate the electrochemical performance of the flake-SnS_2 material for PIBs and the influence of different electrolyte solvents(EC:DEC or EC:DMC:EMC) on the electrochemical performance, the coin cells were assembled and examined by the cyclic voltammetry(CV) and the galvanostatic charge/discharge tests at the voltage range of 0.25—2.35 V. Fig.3(A, B) and Fig.S2(see the Electronic

https://doi.org/10.1007/s40242-021-0017-x

Supplementary Material of this paper) show the initial CV and charge-discharge curves, respectively. During the first discharge process, the peaks at 1.40 V(EC: DEC) and 1.48 V(EC: DMC:EMC) could be attributed to the initial intercalation of K^+ into flake-SnS_2[21,32]. The large irreversible capacity below 1.0 V and peaks located at 0.47 V(EC:DEC) and 0.48 V (EC:DMC:EMC) can be ascribed to the formation of solid electrolyte interphase(SEI), the conversion reaction(from K and SnS_2 to K_xS and Sn), and such conversion reaction of K and SnS_2 to K_xS and Sn, which shifts to above 0.76 V(EC:DEC) and 0.72 V(EC:DMC:EMC) during the second and third cycles[30]. The cathodic peaks at 0.76 V(EC:DEC) and 0.72 V(EC:DMC: EMC) in subsequent cycles could be ascribed to a phase transition process from SnS_2 to K_xS and Sn. After the initial discharge-charge cycle, the CV and charge-discharge curves coincide well, suggesting good electrochemical reversibility. The anodic peaks at 1.15/1.64 V(EC:DEC) and 1.14/1.62 V (EC:DMC:EMC) could correspond to the depotassiation of K-S compounds to SnS_2[21]. Such a reaction process was investigated by XRD as shown in Fig.S3(see the Electronic Supplementary Material of this paper). After the first potassiation, the (101) characteristic peaks of SnS_2 disappear entirely, and the characteristic peaks of K_2S and Sn appear, demonstrating the transformation from SnS_2 to K_2S and Sn. After the first depotassiation, the (101) peak located at 2θ=32.1° reappears with the disappearance of K_2S and Sn peaks, indicating good reversibility of this reaction process. It should be noticed that the absent alloy reaction of Sn and K is due to the high cut-off voltage. Usually, the alloy reaction leads to a huge volume expansion and poor cycling performance[33]. Meanwhile, the high cut-off voltage would avoid the generation of dendritic K, which may cause a potential safety issue. Accordingly, electrochemical tests are conducted in the voltage range of 0.25—2.35 V to promote the electrochemical stability[34]. Fig.3(C) presents the electrochemical reversibility of SnS_2 electrode materials at 100 mA/g. After cycling 30 cycles, a higher capacity conservation rate with a capacity of 312 mA·h/g is obtained in EC:DEC than that in ED:DMC:EMC, indicating favorable electrochemical reversibility in EC:DEC. Fig.3(D) shows the rate ability of the SnS_2. The average specific capacities of 328, 223, 181, 135, and 112 mA·h/g are obtained in EC:DEC at 100, 200, 300, 500, and 800 mA/g, respectively. By comparison, the SnS_2 displays smaller average specific capacities of 295, 168, 145, 99, and 37 mA·h/g under the same condition in the electrolyte with EC:DMC:EMC. When the current density returns to 100 mA/g, a better reversible specific capacity of 206 mA·h/g is gained in EC:DEC than EC:DMC: EMC(105 mA·h/g). These clear differences between the two electrolytes could be attributed to smaller electrochemical impedance and faster K-ion diffusion in EC:DEC[Fig.S4(A), see the Electronic Supplementary Material of this paper]. These results demonstrate SnS_2 material in the electrolyte with EC:DEC possesses higher capacities and reversibility than that with EC:DMC:EMC. Meanwhile, the average discharge potential of SnS_2 electrodes in EC:DEC is 0.6 V[Fig.S4(B), see the Electronic Supplementary Material of this paper], indicating that SnS_2 is an effective anode material for K storage. It also should be noticed that all the electrochemical

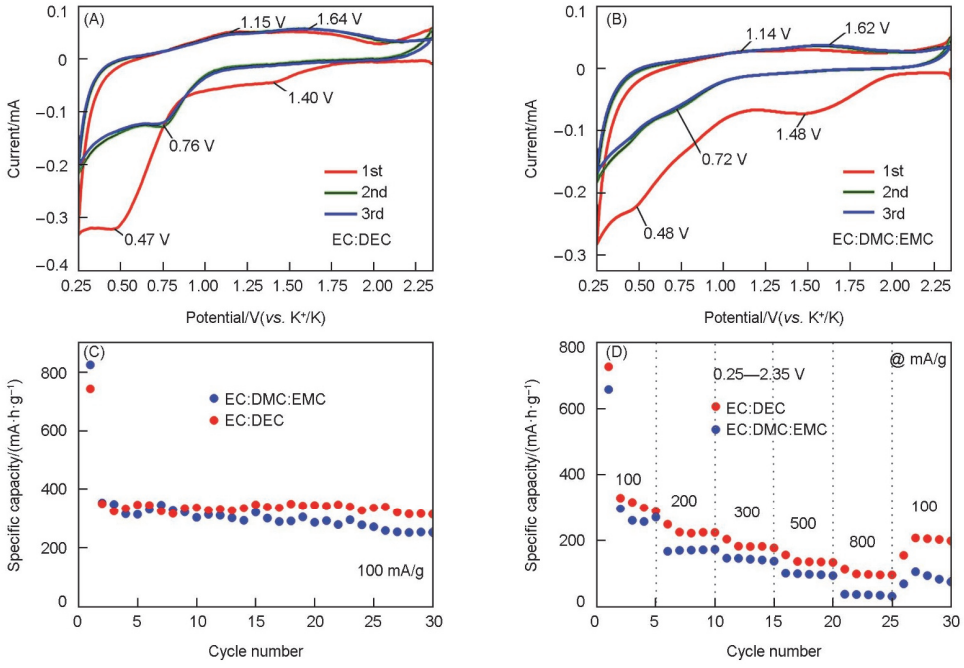

Fig.3 Electrochemical performances of flake-SnS_2 anode for PIBs:CV curves of flake-SnS_2 in EC:DEC based electrolyte(A) and EC:DMC:EMC based electrolyte(B), and cycling property at 100 mA/g(C) and rate performance(D) of flake-SnS_2 in EC:DEC and EC:DMC:EMC based electrolytes, respectively

https://doi.org/10.1007/s40242-021-0017-x

performance is based on the pure SnS_2 without any surface modification. Previous reports suggest that electrochemical performance of SnS_2 could be further improved by carbon coating or composite fabrication. To explore the long cycling performance of the SnS_2, the capacity retention of flake-SnS_2 at 500 mA/g in EC:DEC based electrolytes was obtained(Fig.S5, see the Electronic Supplementary Material of this paper). Before cycling, the cell run three circles as the activation process at 50 mA/g. After 200 cycles, the capacity retention of flake-SnS_2 electrode is 60.3%, demonstrating good cycling stability of the SnS_2 material in EC:DEC based electrolyte. It should be noticed the electrochemical performance of SnS_2 is tested under the common electrolyte system, which could match the cathode materials well. It indicates the potential application of full cell based on the SnS_2.

To uncover the K-ion storage mechanism of SnS_2 in the electrolyte with EC:DEC, kinetic analyses were carried out as shown in Fig.4. Fig.4(A) displays the CV curves at the sweep rates from 0.2 mV/s to 1.0 mV/s. The reaction kinetic is analyzed based on the relationship between peak current(i) and scan rate(v):

$$i = av^b \quad (1)$$

in which b-value is between 0.5 and 1.0. When b=0.5, the reaction process is dominated by semi-linear diffusion[35]. While when b=1.0, the reaction is dominated by the surface capacitive process[36]. As shown in Fig.4(B), the b-value of the anodic peaks of SnS_2 electrodes is about 0.64, suggesting that the reaction process contains two different types of K-ion storage mechanisms. The ratios of the capacity contribution of the two reaction processes can be calculated by using the formula (2):

$$I = k_1 v + k_2 v^{1/2} \quad (2)$$

in which $I(V)$ represents the currents at different sweep rates and a particular potential, v is the scan rate, and the $k_1 v$ and $k_2 v^{1/2}$ indicate currents controlled by capacitive and diffusion behaviors, respectively[37]. At 0.2 mV/s, the CV area(blue) with a capacity ratio of 59.2% dominated by capacitive is displayed in Fig.4(C). As the scan rate is increased, the capacitive contribution ratios largen gradually. When the scan rate reaches 1.0 mV/s, it can be up to 92.7%. This high capacitance contribution rate is attributed to the ultrathin nanosheets morphology of flake-SnS_2, which provides a large contact area between electrode materials and electrolyte and enough K ion storage sites. The above results demonstrate a capacitor-dominated K-ion storage process in the SnS_2 electrodes, further indicating that SnS_2 in the electrolyte with EC:DEC possesses fast reaction kinetic.

The XPS of electrode after the 1st discharge to 0.25 V was carried out to explore the SEI on the flake-SnS_2 material in different electrolytes(EC:DEC and EC:DMC:EMC)(Fig.5). As shown in the Fig.5(A) and (B), the K_{2p} spectra can be divided into K—F, K—O, and K—C bonds on the electrode surface in the two electrolytes, which are the main components of SEI[38,39]. The K—C and K—O bonds come from the decomposition of carbonate electrolyte during cycling[38,39]. The K—F bonds can be attributed to the KPF_6 decomposition. Observing the histogram of the proportion of each potassium component content[Fig.5(C) and (D)], the proportions of K—F and K—O

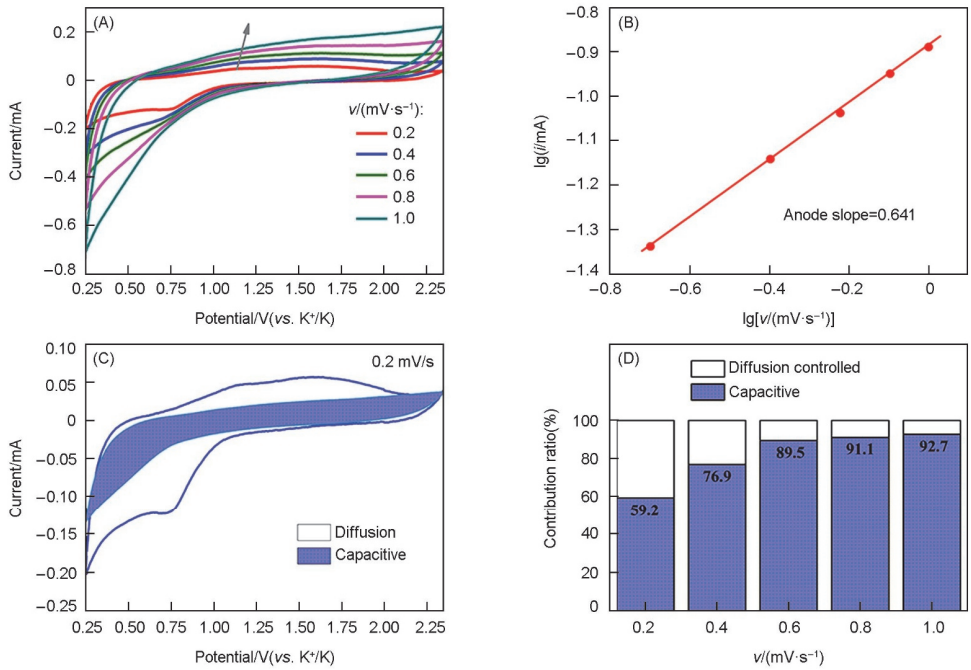

Fig.4 CV curves for flake-SnS_2 electrode in EC:DEC based electrolyte from 0.2 mV/s to 1.0 mV/s(A), linear relationship between lg*i* and lg*v* on the peaks labeled in(A)(B), the typically capacitance contriution(blue region) at 0.2 mV/s(C), and the diffusion and capacitive contribution at different sweep rates for flake-SnS_2 in EC:DEC based electrolyte(D)

https://doi.org/10.1007/s40242-021-0017-x

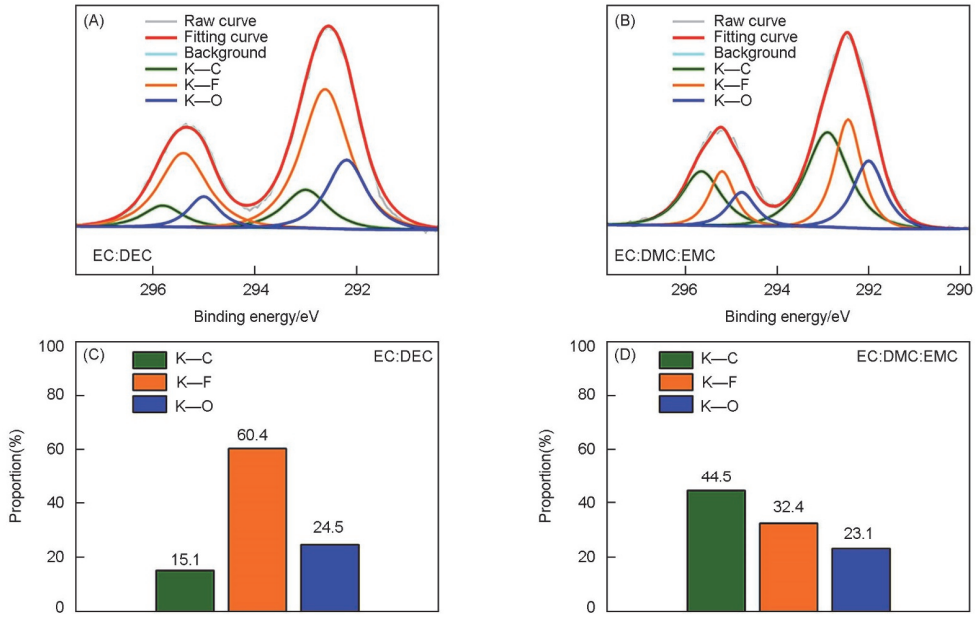

Fig.5 XPS spectra of K_{2p} of flake-SnS_2 in EC:DEC(A) and EC:DMC:EMC(B) based electrolytes after the 1st discharge to 0.25 V and the proportion of each potassium containing component in flake-SnS_2 in EC:DEC(C) and EC:DMC:EMC(D) based electrolytes

bonds increase from 32.4% and 23.1% in EC:DMC:EMC to 60.4% and 24.5% in EC:DEC, respectively. This implies a stronger KF-rich SEI layer on the surface of the flake-SnS_2 in EC:DEC based electrolyte. And the proportion of K—C bonds decreases from 44.5% in EC:DMC:EMC to 15.1% in EC:DEC, indicating that EC:DEC electrolyte is less decomposed during cycling. The above results demonstrate that the surface of the flake-SnS_2 anode in EC:DEC based electrolyte is prone to form a stronger KF-rich SEI layer, and the decomposition of the electrolyte is inhibited to a certain extent. This allows the flake-SnS_2 anode to exhibit better electrochemical performance in EC:DEC based electrolyte.

4 Conclusions

In summary, SnS_2 ultrathin nanosheets are synthesized through a hydrothermal method and employed as anode materials for potassium ion batteries. The optimized electrolyte facilitates to enhance the electrochemical performance of SnS_2. In the optimized EC:DEC electrolyte, SnS_2 displays an enhanced capacity of 312 mA·h/g at 100 mA/g after 30 cycles and improved rate ability. The ex-XRD results demonstrate the K ion storage mechanism of SnS_2 in the voltage range of 0.25—2.35 V. In addition, a capacitor-dominated K-ion storage process in the SnS_2 electrodes is confirmed. This work demonstrates the potential application of SnS_2 as anode materials for the potassium ion batteries.

Electronic Supplementary Material

Supplementary material is available in the online version of this article at http://dx.doi.org/10.1007/s40242-021-0017-x.

Acknowledgements

This work was supported by the National Natural Science Foundation of China (Nos.21805182, 22075171) and the Fundamental Research Funds for the Central Universities of China.

Conflicts of Interest

The authors declare no conflicts of interest.

References

[1] Yao Q., Zhu C., *Advanced Functional Materials*, **2020**, *30*, 2005209
[2] Ding J., Zhang H., Zhou H., Feng J., Zheng X., Zhong C., Paek E., Hu W., Mitlin D., *Advanced Materials*, **2019**, *31*, 1970217
[3] Rajagopalan R., Tang Y., Ji X., Jia C., Wang H., *Advanced Functional Materials*, **2020**, *30*, 1909486
[4] Liang Y., Luo C., Wang F., Hou S., Liou S.-C., Qing T., Li Q., Zheng J., Cui C., Wang C., *Advanced Energy Materials*, **2019**, *9*, 1802986
[5] Ju Z., Zhang S., Xing Z., Zhuang Q., Qiang Y., Qian Y., *ACS Applied Materials & Interfaces*, **2016**, *8*, 20682
[6] Ji Y.-R., Weng S.-T., Li X.-Y., Zhang Q.-H., Gu L., *Rare Metals*, **2020**, *39*, 205
[7] Wang K., Pei S., He Z., Huang L.-A., Zhu S., Guo J., Shao H., Wang J., *Chemical Engineering Journal*, **2019**, *356*, 272
[8] Wang Y.-Y., Zhao Z.-W., Liu Y., Hou L.-R., Yuan C.-Z., *Rare Metals*, **2020**, *39*, 1082
[9] Bai P., Jiang K., Hang X., Xu J., Guo S., Zhou H., *ACS Applied Materials & Interfaces*, **2020**, *12*, 10490
[10] Qi S.-H., Deng J.-W., Zhang W.-C., Feng Y.-Z., Ma J.-M., *Rare Metals*, **2020**, 39, 970
[11] Zhang W., Ming J., Zhao W., Dong X., Hedhili M. N., Costa P. M. F. J., Alshareef H. N., *Advanced Functional Materials*, **2019**, *29*, 1903641
[12] Lei K.-X., Wang J., Chen C., Li S.-Y., Wang S.-W., Zheng S.-J., Li F.-J., *Rare Metals*, **2020**, *39*, 989
[13] Zeng S., Zhou X., Wang B., Feng Y., Xu R., Zhang H., Peng S., Yu Y., *Journal of Materials Chemistry A*, **2019**, *7*, 15774
[14] Liao J., Hu Q., Mu J., He X., Wang S., Jiemin D., Chen C., *Chemical Communications*, **2019**, *55*, 13916

[15] Bin D.-S., Duan S.-Y., Lin X.-J., Liu L., Liu Y., Xu Y.-S., Sun Y.-G., Tao X.-S., Cao A.-M., Wan L.-J., *Nano Energy*, **2019**, *60*, 912
[16] Wang Y., Zhou J., Wang Z., Zhao L., Li P., Yang Y., Yang C., Huang H., Guo S., *Advanced Energy Materials*, **2017**, *8*, 1701648
[17] Zhao J., Zhang Y., Wang Y., Li H., Peng Y., *Journal of Energy Chemistry*, **2018**, *27*, 1536
[18] Chen Q., Sun S., Zhai T., Yang M., Zhao X., Xia H., *Advanced Energy Materials*, **2018**, *8*, 180005
[19] Wang X., Li X., Li Q., Li H., Xu J., Wang H., Zhao G., Lu L., Lin X., Li H., Li S., *Nano-Micro Letters*, **2018**, *10*, 46
[20] Fang L., Xu J., Sun S., Lin B., Guo Q., Luo D., Xia H., *Small*, **2019**, *15*, 1804806
[21] Sun Q., Li D., Dai L., Liang Z., Ci L., *Small*, **2020**, *16*, 2005023
[22] Zhong Y., Liu D., Wang L.-T., Zhu H.-G., Hong G., *Journal of Colloid and Interface Science*, **2020**, *561*, 593
[23] Jana M., Xu R., Cheng X.-B., Yeon J. S., Park J. M., Huang J.-Q., Zhang Q., Park H. S., *Energy & Environmental Science*, **2020**, *13*, 1049
[24] Lv X., Wei W., Huang B., Dai Y., *Journal of Materials Chemistry A*, **2019**, *7*, 2165
[25] Okoshi M., Yamada Y., Komaba S., Yamada A., Nakai H., *Journal of the Electrochemical Society*, **2016**, *164*, A54
[26] Zhang J., Cao Z., Zhou L., Park G.-T., Cavallo L., Wang L., Alshareef H. N., Sun Y.-K., Ming J., *ACS Energy Letters*, **2020**, *5*, 3124
[27] Wang H., Zhai D., Kang F., *Energy & Environmental Science*, **2020**, *13*, 4583
[28] Liu W., Liu P., Mitlin D., *Advanced Energy Materials*, **2020**, *10*, 2002297
[29] Shi X., Yang Z., Liu Y., Tang Y., Liu Y., Gao S., Yang Y., Chen X., Zhong Y., Wu Z., Guo X., Zhong B., *ChemElectroChem*, **2020**, *7*, 4484
[30] Xia J., Jiang K., Xie J., Guo S., Liu L., Zhang Y., Nie S., Yuan Y., Yan H., Wang X., *Chemical Engineering Journal*, **2019**, *359*, 1244
[31] Wang J., Huang J., Huang S., Notohara H., Urita K., Moriguchi I., Wei M., *ACS Sustainable Chemistry & Engineering*, **2020**, *8*, 9519
[32] Liu Y., Kang H., Jiao L., Chen C., Cao K., Wang Y., Yuan H., *Nanoscale*, **2015**, *7*, 1325
[33] Fang S., Shen L., Li S., Kim G.-T., Bresser D., Zhang H., Zhang X., Maier J., Passerini S., *ACS Nano*, **2019**, *13*, 9511
[34] Hu R., Zhu K., Ye K., Yan J., Wang Q., Cao D., Wang G., *Applied Surface Science*, **2021**, *536*, 147832
[35] Yang C., Lv F., Zhang Y., Wen J., Dong K., Su H., Lai F., Qian G., Wang W., Hilger A., Xu Y., Zhu Y., Deng Y., Hu W., Manke I., Chen Y., *Advanced Energy Materials*, **2019**, *9*, 1902674
[36] Suo G., Zhang J., Li D., Yu Q., He M., Feng L., Hou X., Yang Y., Ye X., Zhang L., Wang W., *Journal of Colloid and Interface Science*, **2020**, *566*, 427
[37] Tang Y., Zhao Z., Hao X., Wang Y., Liu Y., Hou Y., Yang Q., Wang X., Qiu J., *Journal of Materials Chemistry A*, **2017**, *5*, 13591
[38] Lei Y., Han D., Dong J., Qin L., Li X., Zhai D., Li B., Wu Y., Kang F., *Energy Storage Materials*, **2020**, *24*, 319
[39] Li L., Fang C., Wei W., Zhang L., Ye Z., He G., Huang Y., *Nano Energy*, **2020**, *72*, 104651